Boron Enriched $RE_2Fe_{14}B$-Base Melt Spun Alloys With Intrinsic Coercivities Over 1000 kA/m

Israel Betancourt, Thomas Schrefl, and Hywel A. Davies

Department of Engineering Materials, University of Sheffield, Sheffield S1 3JD, U.K.

Considerable enhancement of magnetic properties was attained in nanophase $RE_{12}Fe_{82}B_6$-base melt spun alloys ($RE = Nd, Nd+Pr$) by means of B excess content (10 at%) and Zr-Co addition (2% and 7%, respectively). The intrinsic coercivity exhibited a marked improvement (respect to the stoichiometric 6 at% B alloy) within the range 50%–65%, with a maximum of 1161 $\pm$ 14 kA/m for the B-rich and Zr-containing alloy, together with an excellent combination of remanence and energy density values of 0.90 $\pm$ 0.01 T and 137$\pm$4 kJ/m^3, respectively. Further Co addition led to a Curie temperature enlargement (350 °C) preserving high coercivity (1176 $\pm$ 31 kA/m) and useful energy densities (119 $\pm$ 4 kJ/m^3). Results were interpreted on the basis of microstructure and intrinsic magnetic property variations, together with micromagnetic calculations.

Index Terms—**Hard magnetic alloys, high coercivity alloys, micromagnetism.**

I. Introduction

MELT-SPUN rare earth (RE)-iron-boron hard magnetic alloys are the precursor materials for fabrication of isotropic bonded magnets, which can be obtained by blending coercive RE-Fe-B powder with a binder, in order to produce flexible or rigid magnets by means of calendering, injection molding, extrusion, or compression bonding [1], [2]. Major applications of these magnets include: motors (spindle- and stepper-type) and sensors for the media storage, consumer electronics, automotive, and office automation (VCRs, camcorders, printers) and in smaller appliances such as watches, clocks, timer switches, and cameras [1], [3]. Additionally, their superior mechanical properties, net-shape formability, corrosion resistance, and lower cost of production (relative to the powder metallurgy route) ensures for these materials an increasing impact within the growing world bonded magnet market [2], [3]. As it has been well established, the microstructure and magnetic properties of RE-Fe-B alloys are very sensitive to processing and particularly, to the alloy composition [4]–[6]. For melt-spun alloys, the stoichiometric composition (with RE content $\sim$11.7 at%) leads to isotropic alloys with a microstructure comprising uniaxial, randomly oriented particles and typical magnetic properties of intrinsic coercivity ${}_iH_c$ between 700–800 kA/m and maximum energy product $(BH)_{max}$ within the range 110–170 kA/m [4], [5] (depending on the remanence J_r values, since $(BH)_{max}$ scales up proportional to J_r^2 for materials with $\mu_{oi}H_c > J_r/2$ [7], [8]). A reducing grain size distribution leads to an increasing exchange coupling interaction among magnetic moments on the grains surface, which in turn leads to enhanced J_r values (well above the $0.5J_s$ limit expected for non-interacting, uniaxial, randomly oriented particles) together with disadvantageous decreasing ${}_iH_c$ [4], [5], [9]. On the other hand, mixed rare earth (Nd-Pr)-Fe-B-based nanocomposite magnets are of interest both, from the viewpoint of the larger anisotropy constant K_1 for the $Pr_2Fe_{14}B$ phase than for its Nd counterpart (which in fact, affords higher ${}_iH_c$ values [4], [10]–[12] and from the potential economic benefit (i.e., lower cost) of employing Didymium having Nd:Pr ratios that correspond to those that occur naturally in rare earth ores (typically 3-4:1) [13]. In this paper, we present the effect of excess of B and Zr-Co additions on the magnetic properties of stoichiometric, isotropic melt spun (Nd-Pr)-Fe-B alloys.

II. Experimental Procedures

The nanocrystalline $RE_{12}Fe_{82}B_6$, $RE_{12}Fe_{78}B_{10}$, $RE_{12}Fe_{76}Zr_2B_{10}$ and $RE_{12}(Fe_{0.9}Co_{0.1})_{76}Zr_2B_{10}$ ($RE = Nd_{0.75}Pr_{0.25}$) alloy samples were obtained by devitrification annealing (10 min at 700 °C) of initially fully amorphous alloy ribbons produced by melt spinning technique. The microstructure of selected ribbon samples were monitored by X-ray diffractometry. The magnetic properties J_r, ${}_iH_c$ and $(BH)_{max}$ were determined using a VSM with a maximum field of 5 T, while the Curie temperature T_c was measured by means of Magnetic Thermogravimetric Analysis (MTGA). On the other hand, Micromagnetic simulations were carried out by using the time integration of the Landau–Lifshitz–Gilbert equation together with a hybrid finite element /boundary element method [14] on realistic alloy models in the form of cubic structures of $100 \times 100 \times 100$ nm^3 comprising 216 irregular grains in intimate contact, with the following intrinsic magnetic properties: $J_s^{Nd} = 1.61$ T, crystalline anisotropy $K_1^{Nd} = 4.3 \times 10^6$ J/m^3 and exchange constant $A^{Nd} = 7.7 \times 10^{-12}$ for the $Nd_2Fe_{14}B$ phase; and $J_s^{Pr} = 1.56$ T, $K_1^{Pr} = 5.6 \times 10^6$ J/m^3 and $A^{Pr} = 12 \times 10^{-12}$ for the $Pr_2Fe_{14}B$ phase [8]. The Pr substitution by Nd was simulated by means of a linear combination of $Nd_2Fe_{14}B$ and $Pr_2Fe_{14}B$ intrinsic properties, which mimics the compositional variation, e.g., $K_1 = 0.75K_1^{Nd} + 0.25K_1^{Pr}$ (and so on for J_s and A).

III. Results and Discussion

X-ray diffractograms for $RE_{12}Fe_{82}B_6$, $RE_{12}Fe_{78}B_{10}$ and $RE_{12}(Fe_{0.9}Co_{0.1})_{76}Zr_2B_{10}$ alloys are shown in Fig. 1. All the peaks present correspond to the tetragonal $RE_2Fe_{14}B$ phase, as is expected from the alloy stoichiometric 12 at% RE content. Same peak distribution was observed for the $RE_{12}Fe_{76}Zr_2B_{10}$ alloy sample. The mean grain sizes d_g for the whole alloy

Digital Object Identifier 10.1109/TMAG.2008.2001524

TABLE I
MAGNETIC PROPERTIES OF $RE_{12}Fe_{82}B_6$-BASED ALLOYS

B content (alloy addition)	$_iH_c$ (kA/m)	J_r (T)	J_s (T)	$(BH)_{mx}$ (kJ/m^3)	T_c (^{o}C)	d_g (nm)	$_iH_c$* (kA/m)	J_r/J_s*
6%	792 ± 15	0.98 ± 0.02	1.47 ± 0.02	146 ± 6	307	35 ± 3	1050	0.61
10%	842 ± 10	0.91 ± 0.01	1.39 ± 0.02	129 ± 3	307	43 ± 6	1082	0.61
10% (Zr)	1161 ± 14	0.90 ± 0.01	1.38 ± 0.03	137 ± 4	282	34 ± 3	1576	0.60
10% (Zr, Co)	1176 ± 31	0.83 ± 0.01	1.31 ± 0.02	119 ± 4	350	58 ± 6	1512	0.60

$RE = Nd_{0.75}Pr_{0.25}$. Micromagnetic data (*) for the corresponding alloy models

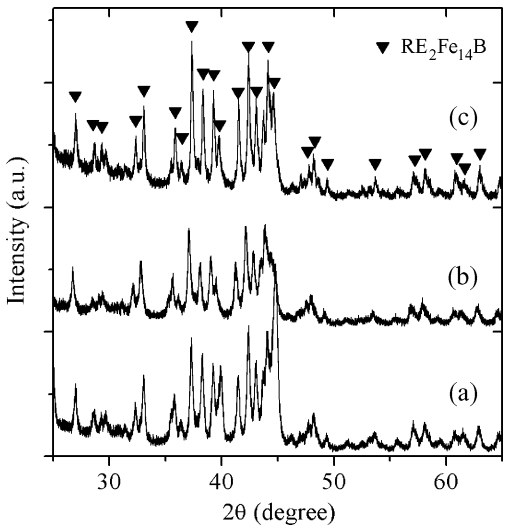

Fig. 1. X-ray diffractograms for: (a) $RE_{12}Fe_{82}B_6$; (b) $RE_{12}Fe_{78}B_{10}$; and (c) $RE_{12}(Fe_{0.9}Co_{0.1})_{76}Zr_2B_{10}$ alloys.

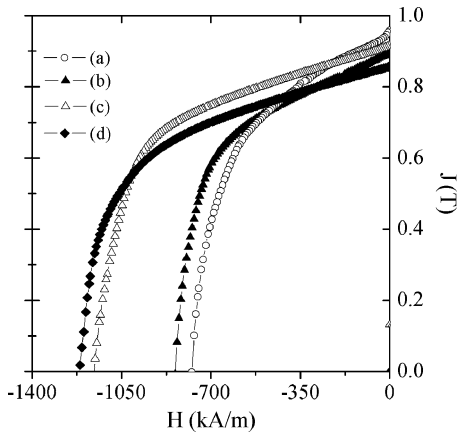

Fig. 2. Demagnetising J(H) curves for: (a) $RE_{12}Fe_{82}B_6$; (b) $RE_{12}Fe_{78}B_{10}$; (c) $RE_{12}Fe_{76}Zr_2B_{10}$; and (d) $RE_{12}(Fe_{0.9}Co_{0.1})_{76}Zr_2B_{10}$ alloys.

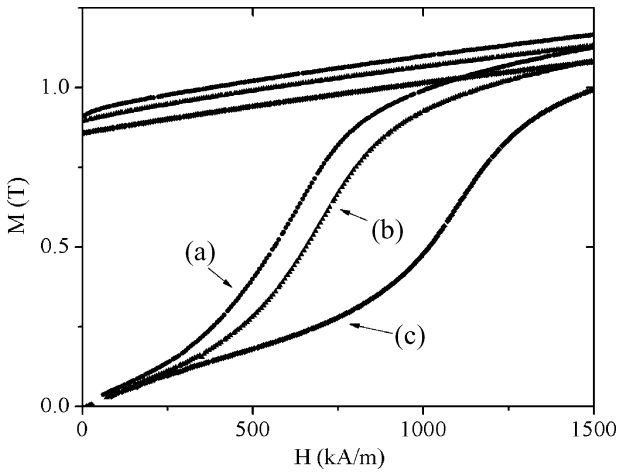

Fig. 3. Initial magnetization curves for: (a) $RE_{12}Fe_{82}B_6$; (b) $RE_{12}Fe_{78}B_{10}$; and (c) $RE_{12}Fe_{76}Zr_2B_{10}$ alloys.

series, determined by means of the Scherrer formula on at least five different peaks, are displayed in Table I.

Curie temperatures for the whole alloy series are shown in Table I. For the initial $RE_{12}Fe_{82}B_6$ ribbon sample, T_c was of 307 °C, which is slightly lower than the reported 310 °C of the $Nd_2Fe_{14}B$ hard phase [15]. This reduced T_c can be attributed to the minor T_c of the $Pr_2Fe_{12}B$ phase compared with its $Nd_2Fe_{14}B$ counterpart [15]. Same T_c value was observed for the boron enriched $RE_{12}Fe_{78}B_{10}$ alloy, which would imply that the excess of B is segregating outside the 2/14/1 grains and forming a secondary phase, likely an iron-boride, as suggested in [16] for equivalent B-rich RE-Fe-B ribbons. A significant T_c reduction is exhibited for the Zr doped ribbon sample (282 °C) due to the deleterious effect of the incorporation of Zr atoms into the $RE_2Fe_{14}B$ unit cell [17], [18], followed by a remarkable T_c improvement (up to 350 °C) for the Co-substituted alloy, reflecting the stronger Fe-Co exchange interactions [4], [5], [15]. Demagnetising J(H) curves for all the alloy ribbons are shown in Fig. 2, for which an increasing trend of $_iH_c$ is observed with the composition sequence shown in Table I, starting at 792 ± 15 kA/m for the reference $RE_{12}Fe_{82}B_6$ alloy, to a maximum of 1176 ± 31 kA/m for the $RE_{12}(Fe_{0.9}Co_{0.1})_{76}Zr_2B_{10}$ ribbon sample. On the other hand, J_r exhibited a monotonous diminishing tendency across the alloy series, from 0.98 ± 0.02 T to 0.83 ± 0.01. The highest $(BH)_{max}$ value for the B-enriched alloys corresponded to the $RE_{12}Fe_{76}Zr_2B_{10}$ ribbon sample (137 kJ/m^3).

The diminishing tendency observed for the saturation magnetization J_s should be attributed to the progressive reduction in Fe content, since all the composition variation were realized by Fe substitution. The marked reduction in J_s after B content increment up to 10 at%, causes a diminished initial susceptibility, as is shown in Fig. 3, for which the initial magnetization curve displays a lower slope for the $RE_{12}Fe_{78}B_{10}$ alloy ribbon, relative to the reference $RE_{12}Fe_{82}B_6$ alloy.

The high energy density of the stoichiometric alloy (146 ± 6 kJ/m^3) results from its high remanence value, which in turn, is afforded by the small d_g (35 nm ± 3 nm, Table I). In spite of the decreasing J_r observed for the B enriched alloys, $(BH)_{max}$

maintains above 120 kJ/m^3 for the $RE_{12}Fe_{78}B_{10}$ alloy ribbon, and even increases up to 137 kJ/m^3 for the $RE_{12}Fe_{76}Zr_2B_{10}$ alloy. This latter value is a consequence of the improved squareness in the second J(H) quadrant (see Fig. 2), which results from an homogeneous and refined grain size distribution (34 ± 3 nm). For the Co-containing alloy, the noticeable grain size coarsening (up to 58 ± 6 nm) besides the reduced J_s, causes a significant J_r decrement and thus, the lowest maximum energy product (119 ± 4 kJ/m^3) of the studied alloy series. On the other hand, the initial increment of ${}_iH_c$ for the $RE_{12}Fe_{78}B_{10}$ alloy (respect to the $RE_{12}Fe_{82}B_6$ sample) can be explained as follows: after the nucleation of the reversed domain at energy favorable regions for magnetization reversal (such as grain boundaries with deteriorated magnetic properties, coupled grains, or misaligned grains [7], [8]), its further propagation throughout the grains is hindered at the secondary particles afforded by the excess of B. This secondary minor phase would be present in a volume fraction lower than the detection limit of the XRD technique ($<$ 5%). The further ${}_iH_c$ enhancement after Zr addition is in accord with previous reports on $Nd_{12}Fe_{82-x}Zr_xB_6$ alloys [17], [19], for which higher anisotropy fields H_A were reported as a result of the replacing of Nd atoms by Zr within the $RE_2Fe_{14}B$ unit cell [17], [18]. This Zr entering to the 2/14/1 cell is also reflected by the considerable reduction in T_c determined for the $RE_{12}Fe_{76}Zr_2B_{10}$ alloy sample (see Table I). Additionally, the enhancement of H_A indicates an enlarged anisotropy constant, which in turn, causes a decreased initial susceptibility, as it is shown in Fig. 3, for which the initial magnetization curve for the $RE_{12}Fe_{76}Zr_2B_{10}$ alloy sample exhibits a lower slope, relative to $RE_{12}Fe_{82}B_6$ and $RE_{12}Fe_{78}B_{10}$ ribbons. Finally, although the $RE_{12}(Fe_{0.9}Co_{0.1})_{76}Zr_2B_{10}$ alloy sample exhibits a slight ${}_iH_c$ improvement respect to the $RE_{12}Fe_{76}Zr_2B_{10}$ ribbon (of $\sim$1.2% only), when the error intervals are considered for both samples, the ${}_iH_c$ becomes very similar. According to previous reports, Co addition in $Nd_{12}Fe_{14}B_6$ alloys decreases the H_A, which in fact, leads to reduced ${}_iH_c$ values [4], [5], [15]. This implies for the present case, that a small Zr addition is able to counterbalance the deleterious effect of the Co substitution on H_A, with a concomitant beneficial T_c increment (up to 350 °C, Table I).

Micromagnetically simulated J(H) curves are shown in Fig. 4 for the whole alloy series. For the initial $RE_{12}Fe_{82}B_6$ alloy model, an ${}_iH_c$ of 1050 kA/m was observed, which is considerable higher (35%) than the experimental value, due to the fact that the cubic alloy model assumes the ideal nucleation field for reverse domains. This difference between theoretical ${}_iH_c$ values and experimental data is known as the Brown's paradox [7], [8]. Nevertheless, the simulated J(H) plot reflects the intergranular exchange coupling, with a J_r/J_s ratio (0.61) similar to the measured J_r/J_s (of 0.65). Although consistently higher ${}_iH_c$ values were obtained compared with the experimental curves for the remaining alloy models, a progressive ${}_iH_c$ enhancement equivalent to the increasing sequence displayed in Table I was attained by assuming for the micromagnetic models, the same experimental microstructural and intrinsic magnetic properties variations observed previously: First, we include for the B-enriched $RE_{12}Fe_{78}B_{10}$ alloy model, the presence of magnetic Fe_3B grains as secondary phase in a volume fraction of 2%, which according to [16] are feasible to form as a consequence of the excess of B content. This model showed an ${}_iH_c$ enhancement of 3%, which is similar to the experimentally determined improvement of 6% (see Table I). The difference in ${}_iH_c$ improvement should be ascribed to the grain coarsening effect after B enrichment, which was not included into the micromagnetic model. Additionally, a comparable J_r/J_s enhancement was obtained.

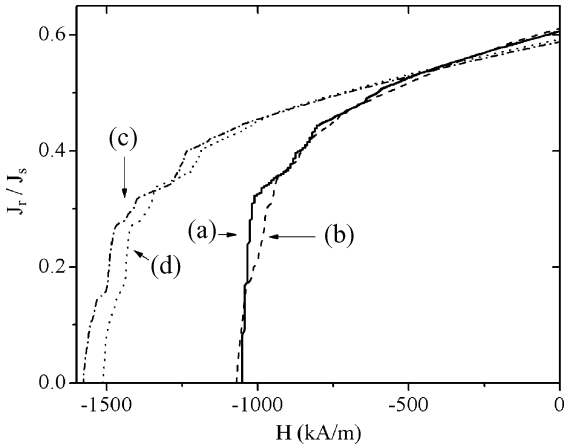

Fig. 4. Micromagnetically simulated J(H) curves for: (a) $RE_{12}Fe_{82}B_6$; (b) $RE_{12}Fe_{78}B_{10}$; (c) $RE_{12}Fe_{76}Zr_2B_{10}$; and (d) $RE_{12}(Fe_{0.9}Co_{0.1})_{76}Zr_2B_{10}$ compositions.

On the other hand, for the $RE_{12}Fe_{76}Zr_2B_{10}$ alloy model, its intrinsic magnetic properties were changed on the basis of experimental reports on Zr substituted Nd-Fe-B and Pr-Fe-B alloys [17] which include higher K_1 values (estimated from 23.8% higher H_A) and reduced J_s and A (took from -1.56% lower J_s and -2.17% smaller T_c, respectively). These adjusted intrinsic parameters led to an ${}_iH_c$ enlargement of 41% (respect to the $RE_{12}Fe_{78}B_{10}$ alloy model), which was very close to the 38% experimentally determined from Fig. 2. Finally, for the Co-containing composition, a reduced K_1 value (estimated from -2.2% diminished H_A) with concurrent J_s and A improvements (determined from 0.52% enhanced J_s and 14.6% higher T_c, respectively) were considered according to experimental reports [17], [21], [22], which resulted in an effective ${}_iH_c$ drop of -4% respect to the $RE_{12}Fe_{76}Zr_2B_{10}$ alloy model. This assumption does not include the grain size coarsening observed for the $RE_{12}(Fe_{0.9}Co_{0.1})_{76}Zr_2B_{10}$ alloy, which also plays a determinant role in preserving high intrinsic coercivity values.

ACKNOWLEDGMENT

The work of I. Betancourt was supported in part by Research Grant 56721 Conacyt-Mexico and by a scholarship from DGAPA-UNAM, Mexico. I. Betancourt would like to thank the valuable technical assistance from L. Baños, G. Lara, and E. Fragoso.

REFERENCES

[1] K. H. J. Buschow, "Magnets: Bonded permanent magnets," in *Concise Encyclopedia of Magnetic & Superconducting Materials*, K. H. J. Buschow, Ed., 2nd ed. Amsterdam, The Netherlands: Elsevier, 2005, pp. 858–862.

[2] S. Rivoirard and D. Givord, "Hard-magnetic nanostructures," in *Advance Magnetic Nanostructures*, D. Sellmyer and R. Skomski, Eds. New York: Springer, 2006, p. 355.
[3] P. Campbell, D. N. Brown, Z. M. Chen, P. C. Guschl, D. J. Miller, and B. M. Ma, " $R_2Fe_{14}B$-type isotropic powders for bonded magnets," in *Proc. 18th Int. Workshop High Perform. Magnets Their Appl.*, 2004, pp. 67–76.
[4] G. C. Hadjipanayis, J. F. Liv, A. Gabay, and M. Marinescu, "Current status of rare-earth permanent magnet research in USA," in *Proc. 19th Int. Workshop Rare Earth Permanent Magnets Their Appl.*, Beijing, 2006, pp. 12–20.
[5] S. Hirosawa, "Magnets: Remanence-enhanced," in *Concise Encyclopedia of Magnetic & Superconducting Materials*, K. H. J. Buschow, Ed., 2nd ed. Amsterdam, The Netherlands: Elsevier, 2005, pp. 877–.
[6] M. J. Kramer, L. H. Lewis, Y. Tang, K. W. Dennis, and R. W. McCallum, "Microstructural refinement in melt-spun $Nd_2Fe_{14}B$," *Scrip. Mater.*, vol. 47, pp. 557–562, 2002.
[7] H. Kronmuller, R. Fischer, M. Seeger, and A. Zern, "Micromagnetism and microstructure of hard magnetic materials," *J. Phys. D: Appl. Phys.*, vol. 29, pp. 2274–2280, 1996.
[8] H. Kronmuller and M. Fahnle, *Micromagnetism and the Microstructure of Ferromagnetic Solids*. Cambridge, U.K.: Cambridge University Press, 2003, pp. 90–91.
[9] H. A. Davies, "Nanocrystalline exchange enhanced hard magnetic alloys," *J. Magn. Magn. Mater.*, vol. 157/158, pp. 11–15, 1996.
[10] D. Goll, M. Seeger, and H. Kronmuller, "Magnetic and microstructural properties of nanocrystalline exchange coupled PrFeB," *J. Magn. Magn. Mater.*, vol. 185, pp. 49–55, 1998.
[11] G. Mendoza and H. A. Davies, "The coercivity of nanophase melt spun PrFeB alloys," *J. Alloys Comp.*, vol. 281, pp. 17–21, 1998.
[12] H. A. Davies, J. I. Betancourt, and C. L. Harland, "Nanophase $(Nd/Pr)_2Fe_{14}B/\alpha - Fe$ alloys- Attractive materials for isotropic magnets with enhanced properties," *Scrip. Mater.*, vol. 44, pp. 1337–1341, 2001.
[13] M. Okada, S. Sugimoto, C. Ishizaka, T. Tanaka, and M. Homma, "Didymium-Fe-B sintered permanent magnets," *J. Appl. Phys.*, vol. 57, pp. 4146–4150, 1985.
[14] J. Fidler and T. Schrefl, "Micromagnetic modeling: The current state of the art," *J. Phys. D: Appl. Phys.*, vol. 33, pp. R135–R145, 2000.
[15] J. F. Herbst, " $R_2Fe_{14}B$ materials: Intrinsic properties and technological aspects," *Rev. Mod. Phys.*, vol. 63, pp. 819–840, 1991.
[16] H. W. Chang, W. C. Chang, J. C. Ho, W. M. Hikal, and H. H. Hamdeh, "Magnetic properties and Mossbauer studies of $Pr_yFe_{90-y}B_{10}(y = 8 - 11.76)$ nanocomposites," *Phys. B*, vol. 327, pp. 292–297, 2003.
[17] M. Jurczyk and W. E. Wallace, "Magnetic behavior of $R_{1.9}Zr_{0.1}Fe_{14}B$ and $R_{1.9}Zr_{0.1}Fe_{12}Co_2B$," *J. Magn. Magn. Mater.*, vol. 59, pp. L182–L186, 1986.
[18] T. W. Capehart, R. K. Mishra, and F. E. Pinkerton, "Determination of the Zr site in Zr-substituted $Nd_2Fe_{14}B$," *J. Appl. Phys.*, vol. 73, pp. 6476–6480, 1993.
[19] J. I. Betancourt and H. A. Davies, "High coercivity Zr and Co substituted (Nd-Pr)-Fe-B nanophase hard magnetic alloys," *IEEE Trans Magn.*, vol. 37, pp. 2480–2483, 2001.
[20] P. de Rango, F. N. Genin, D. Fruchart, A. Traverse, S. Rivoirard, and I. Popa, "Localisation of Zr in Nd-Fe-B alloys," *J. Magn. Magn. Mater.*, vol. 226–230, pp. 1377–1378, 2001.
[21] C. Abache and H. Oesterreicher, "Structural and magnetic properties of $R_2Fe_{14-x}T_xB$ ($R = Nd$, Y; $T = Cr$, Mn, Co," *J. Appl. Phys.*, vol. 60, pp. 1114–1117, 1986.
[22] R. Grossinger, R. Krewenka, X. K. Sun, R. Eibler, H. R. Kirchmayr, and K. H. J. Buschow, "Magnetic phase transitions and magnetic anisotropy in $Nd_2Fe_{14-x}Co_xB$ compounds," *J. Less-Comm Metals*, vol. 124, pp. 165–170, 1986.

Manuscript received February 28, 2008. Current version published December 17, 2008. Corresponding author: I. Betancourt (e-mail: israelb@correo.unam.mx).